

1 **Effect of Solar Radiation on Suspension Bridge** 2 **Performance**

3 **Robert Westgate¹; Ki-Young Koo²; and James Brownjohn³.**

4 5 **Abstract**

6 Observations on a UK suspension bridge show that thermal expansion and contraction cycles
7 do not follow simple linear relationships with a single temperature value, and that time lag
8 and temperature distribution can be significant factors. In this investigation these effects are
9 explored by simulating the transient thermal and quasi-static response of the Tamar Bridge
10 with separate finite element models of the bridge and suspension cables. Thermal loads are
11 determined by calculated solar radiation intensities and temperature data from the bridge
12 monitoring system. Since cloud cover plays an important role to the levels of solar radiation,
13 cloud coverage was estimated indirectly using monitored temperature differences between the
14 top and bottom of the suspended structure. The results demonstrated that peak temperatures
15 of the suspended structure and cables occurred at different times. The lag was caused by
16 differing material properties and the surfaces' ability to absorb and lose heat. Transient
17 phenomena manifest in the structural responses such as the tower sway.

¹Research associate, Department of Civil and Structural Engineering, the University of
Sheffield, Sheffield, United Kingdom, S1 3JD. Email: rjwestgate@gmail.com

²Lecturer, College of Engineering, Mathematics and Physical Sciences, University of Exeter,
Exeter, United Kingdom, EX4 4QF. Email: dr.ki.koo@gmail.com

³Professor of Structural Dynamics, College of Engineering, Mathematics and Physical
Sciences, University of Exeter, Exeter, United Kingdom, EX4 4QF (corresponding author).
Email: j.brownjohn@exeter.ac.uk

18 **Subject headings**

19 cable-stayed bridges; solar radiation; steel; structural health monitoring; suspension bridges;
20 temperature effects

21 **Introduction**

22 One of the many purposes of a Structural Health Monitoring (SHM) system is to look for
23 anomalies in monitored performance data that may signal a change in the structure's
24 condition. A major challenge with this approach is data normalisation, filtering out the
25 contributions of varying operational and environmental loading conditions to reveal
26 underlying effects of structural changes (Sohn 2007). For long span bridges two of the major
27 factors in performance are air temperature and solar radiation, resulting in structural
28 temperature variations with time and location. These in turn cause the structure to expand and
29 deform (Ding and Li 2011b; Ni et al. 2007), as well as drive changes in the material
30 properties, primarily stiffness (Peeters and De Roeck 2001).

31 While data-driven approaches to the data normalisation problem fit mathematical
32 models to recorded deformations and temperatures (Cross et al. 2011), the models cannot
33 recreate the full range of structural responses observed. There is a wider range of possible
34 responses on complex structures such as suspension bridges; variations in structural
35 temperatures produce a variety of deformed configurations. Some of these responses are
36 caused by transient effects and are dependent on how rapidly the structure warms up and
37 cools down.

38 Different regimes of thermal loading will also be experienced through an annual
39 cycle: solar radiation intensities and directions differ seasonally, and air temperatures are
40 lower during winter than in summer. As a result the structure behaves differently throughout
41 the year, such as thermal displacements of the bridge and changes in its modal properties.

42 These seasonal structural responses have only been observed through a results collected from
43 long-term monitoring systems (Ding and Li 2011a; Liu et al. 2009; Miao et al. 2011; Ni et al.
44 2007; Xu et al. 2010; Zhou et al. 2010) and not via mathematical models, to the authors'
45 knowledge.

46 Before transient thermal response mechanisms were studied closely by structural
47 engineers, temperature effects were represented through a series of empirical equations
48 (Churchward and Sokal 1981; Hirst 1984), using thermal loads as variables. However their
49 application is limited to bridges of a similar construction and climate to those studied. Ho and
50 Liu (1989) were among the first to explore transient thermal loads. They used 207 days of
51 data monitored from a concrete bridge in Hong Kong and calibrated a simulated response
52 provided by a one dimensional finite difference model. There are a few other studies that
53 have considered the thermal response of a concrete structure (Minhoto et al. 2005; Moorty
54 and Roeder 1992; Xia et al. 2011). These investigations commented on the temperature
55 gradient through the structure's depth, and attributed thermal lag between the top and bottom
56 faces to the shading of the structure and the low thermal conductivity of concrete.

57 Several studies have observed the thermal response of steel structures. Tong et al.
58 (2001, 2002) performed sensitivity studies on a numerical model to determine the material
59 properties of a steel box section and observed how the temperature gradient was affected by
60 various beam profiles. Cao et al. (2010) identified a temperature gradient through the deck of
61 the Zhanjiang Bay (cable stay) Bridge from results collected by their monitoring system. The
62 effect of heat flow on suspension bridge spans and abutment has been previously studied by
63 Xia et al. (2013). Their investigation uses results collected from Tsing-Ma Bridge during a
64 single day, both from monitored data and finite element (FE) models.

65 As remarked in the Tsing-Ma Bridge investigation, from the thermal response
66 viewpoint a suspension bridge is a much more complex system than a bridge that is only

67 supported on its underside by a truss or girder. The various members have different thermal
68 responses due to their various material properties, shape and size, as well as their location in
69 the structure. Structural responses are also coupled, making it difficult to link specific causes
70 and effects: cable slackening could be caused by thermal expansion or relative movement
71 between deck and tower(s). Multiple structural arrangements further complicate analysis due
72 to structural redundancy and complex shading.

73 In this investigation time dependent thermal effects are studied by examining long-
74 term monitored responses and FE transient analyses from the Tamar Bridge, a suspension
75 bridge with additional stay cables in Southwest England. Transient thermal effects are
76 analysed for 5 days in each of the 12 months of a single year, rather than for a single day.
77 This approach should cover seasonal effects on the thermal response, resulting from differing
78 ranges of air temperature and applied solar radiation.

79 **Application to the Tamar Bridge**

80 **Tamar Bridge**

81 The Tamar Bridge was opened in 1961 and forms the main transport link between Plymouth
82 and Saltash. The bridge has a 335m main span and two 114m side spans, with the deck
83 located halfway up the 73.2m tall concrete towers and supported by a pair of 38cm diameter
84 suspension cables, each consisting of thirty-one 60mm diameter locked-coil steel ropes. A
85 strengthening and widening exercise was completed in 2001, replacing the original concrete
86 deck with a lighter orthotropic steel deck. Furthermore two additional lanes were cantilevered
87 from the 4.9m deep stiffening truss to increase the width of the bridge from 15.2m to 27.2m.
88 These were originally intended to carry traffic during the deck replacement but now serve to
89 provide an additional vehicle lane on one side of the bridge and a footpath and cycleway on
90 the other. Nine pairs of stay cables were also installed as part of the scheme and are arranged

91 as shown in Figure 1. Eight pairs (S3, S1... P3) are attached from the tops of the main towers
92 to either the base of the side towers or the truss. The ninth pair of stay cables is attached to
93 the underside of the truss.

94 The bridge span is able to expand longitudinally due to an expansion gap near the
95 Saltash main towers. Lateral sway of the truss between the main towers is restrained by a pair
96 of thrust bearings, and pairs of rockers at the end of the truss are seated on ledges at the
97 towers to provide vertical restraint to the ends of the spans.

98 **Monitoring systems**

99 The SHM research on the Tamar Bridge has made extensive use of environment and response
100 data provided by a range of structural monitoring systems. The following section describes
101 the systems used in the studies for this paper.

102 *Fugro Monitoring System*

103 Alongside the strengthening and widening scheme, a monitoring system was installed by
104 Fugro Structural Monitoring, allowing the bridge operators to keep track of the bridge's
105 performance. The system consists of 90 data channels from a wide variety of sensors that are
106 detailed in full by Koo et al. (2012), but only the thermogauges are relevant to the
107 investigation in this paper. The locations of these sensors are shown in Figure 1.

108 Six thermogauges are located at midspan that measure the temperature of the deck
109 and the truss: four surround one of the lower spanwise members in the truss, one measures
110 the deck temperature and another measures the temperature of the air underneath the deck.
111 Both of the side spans have a single thermogauge attached to the underside of the deck, as
112 well. Since the system is a retrofit, the sensor that determines the suspension cable
113 temperature is attached to the northern cable wrapping. The local air temperature is acquired
114 from a sensor attached to a hanger near the Saltash tower. The sensors on the cable and

115 suspended structure consist of platinum resistance thermometers mounted on stainless steel
116 shim, which is held against the structure by an adhesive. The air temperature sensor is a
117 ceramic element contained within a stainless steel sheath, protected by a radiation shield.

118 The data from the Fugro system are stored as a comma-delimited ASCII file for each
119 day and are stored on a robust ‘Toughbook’ laptop located in a closed off control chamber.
120 The Toughbook is connected to the internet via an ADSL router, so any changes to the
121 configuration of the sensors can be made by remote connection (Teamviewer or Remote
122 Desktop). The Toughbook transfers the data files every 24 hours via FTP to a server at the
123 University of Exeter, which runs MATLAB scripts to upload and process the recent
124 measurements, and are subsequently added to a MySQL database.

125 ***Webcam***

126 Two webcams are positioned on the top of the Plymouth tower; one pointed towards the
127 Plymouth side span, the other directed towards the main span. Both webcams capture an
128 image of their side of the bridge every 10 minutes to provide visual information of the
129 weather and traffic activity. Similar to the data from the Fugro system, these images are
130 saved to the Toughbook then transferred to a server by FTP.

131 ***Quasi-static displacements***

132 In order to track the structural movements of the bridge, a Total Positioning System (TPS)
133 with a Robotic Total Station (RTS) and 15 reflectors was installed in September 2009 (Koo et
134 al. 2010). The RTS is an innovation of the project, since it is an automated system that locates
135 the reflectors in a cycle within a ten minute duration, repeated at intervals of approximately
136 30 minutes. The RTS provides reflector coordinates in the three axes that characterise the
137 deformation of the bridge. Reflectors are distributed evenly along the southern cantilevered
138 lane of the bridge as well as on the saddle and deck levels of the towers; their locations have

139 also been represented in Figure 1.

140 The RTS unit is a Leica TCA1201, which is designed for measuring at ranges
141 exceeding 8km under ideal weather conditions, and has an accuracy of 2mm plus 2mm per
142 kilometre when measuring distance. For the Tamar Bridge the farthest reflector is 650m from
143 the RTS, so the error over this distance may be up to 3.3mm (2mm plus 1.3mm). The
144 accuracy of the theodolite component of the RTS is 1 arc-second leading to 3.2mm error in
145 the vertical and lateral directions. The RTS is capable of working reliably within the glass
146 housing used for weather protection but there are occasions when poor weather conditions
147 such as morning mist compromise the operation of the system due to light refraction in water
148 droplets. Otherwise the measurements have been reliable.

149 GeoMos Monitor software is installed on the Toughbook to adjust control settings and
150 the periodic measurements of the TPS runs. The software stores the measurements from the
151 RTS in a Microsoft Structured Query Language (MS SQL) database. Subsequently a
152 MATLAB script on the university server reads the data from the Toughbook database and
153 writes it to the MySQL database on the server.

154 One of the pioneering abilities of the SHM system is that the real-time performance of
155 bridge can be viewed online from anywhere in the world with a web browser (Koo et al.
156 2011). This is made possible by a web interface that has access to the MySQL database at the
157 university, which provides the capability of viewing time series of the bridge and weather
158 behaviour and making direct comparisons between two or more sets of data. The web
159 interface has enabled easy manipulation of graphs online to consider how the thermal
160 performance of monitored members may be interacting with each other over long periods of
161 time.

162 **Heat transfer analysis**

163 The wealth of monitored temperature data and webcam images collected from the bridge
164 enable observations on the heat and cloud conditions for each day. This information provides
165 an insight on the structure's ability to gain and lose heat, which can be used calibrate
166 mathematical models so that they replicate monitored behaviour. The equations in the
167 following subsection dictate how heat is transferred within the system.

168 **Heat transfer equations**

169 The temperature field T of a cross section at time t may be expressed by Poisson equation
170 models for the 3D transient heat flow process (Minhoto et al. 2005), representing the heat
171 travelling through a homogenous solid via conduction:

$$k \left(\frac{\partial^2 T}{\partial x^2} + \frac{\partial^2 T}{\partial y^2} + \frac{\partial^2 T}{\partial z^2} \right) = \rho c \frac{\partial T}{\partial t} \quad (1)$$

172 where x , y and z are Cartesian coordinates on the bridge, k the thermal conductivity, ρ
173 the density and c the specific heat capacity of the material.

174 At a boundary the heat flow in a direction normal to the surface is expressed as

$$k \frac{\partial T}{\partial n} + q = 0 \quad (2)$$

175 where n is the normal to the boundary's surface and q is the heat flow at the boundary. For a
176 bridge surface q consists of convection q_c , thermal radiation emitted from the surface q_r and
177 solar irradiation q_j (Branco and Mendes 1993; Elbadry and Ghali 1983):

$$q = q_c + q_r + q_j \quad (3)$$

178 The heat flow caused by convection leaving the surface q_c is determined by:

$$q_c = h(T_{sur} - T_{air}) \quad (4)$$

179 where T_{sur} and T_{air} are the surface and air temperature respectively, and h the convection
180 coefficient. The heat radiated from the surface q_r is dependent on its emissivity coefficient ε
181 :

$$q_r = \varepsilon\sigma T^4 \quad (5)$$

182 where σ is the Stefan-Boltzmann constant, which is the total energy radiated from a black
183 body per unit surface area, per unit time.

184 Finally the amount of solar radiation absorbed by a bridge surface (Minhoto et al.
185 2005; Xia et al. 2013) is

$$q_j = -\alpha J_0 \quad (6)$$

186 where α is the solar radiation absorption coefficient of the surface material (between 0 and
187 1), and J_0 is the total daily irradiance on the bridge surface. An estimate for the solar
188 radiation for any day of the year was calculated using the Johnson-Woodward model
189 (Johnson et al. 1995; Woodward et al. 2001), which was originally intended for agricultural
190 purposes. The model was chosen due to recommendation by Rivington et al. (2005) and for
191 its simplicity. The formulae used to calculate the radiation are found in the Appendix.

192 **Estimation of cloud cover**

193 In order to approximate the intensity of solar radiation on the deck, values for the cloud cover
194 at the observed time are required. Cloud-cover has not been well studied in the bridge
195 community, but it affects the amount of solar radiation the surface of the bridge deck receives
196 directly. While data were available from Plymouth Airport (Roborough), the data were

197 inadequate, as elaborated later. Thus an alternate method was developed with the aim that FE
198 simulated structural temperatures would be similar to the monitored values.

199 Two dates with varying cloud levels were chosen to gauge upper and lower bounds
200 for the calculated cloud cover values. Webcam images contain several features that indicate
201 the degree of cloud cover: images with cloudier skies are greyer and less bright than images
202 on clear days. Shadows also have crisp edges when they are under direct sunlight. In future,
203 image processing software might be trained to identify such features. For the investigation the
204 lower bound was January 10th, 2010, when the bridge was covered by fog for the duration of
205 the day. The upper bound was July 8th, 2010, as the images indicated a clear day throughout
206 the morning.

207 Another readily available indicator for the amount of cloud cover is the comparison of
208 temperature data from two or more sensors on the structure, such as the time series in Figure
209 2. On cloudy days like January 10th 2010 (top) the temperature of the deck, cables and truss is
210 very similar throughout the day, since the bridge is mostly warmed by the air. On clear days
211 such as July 8th 2010 (bottom) the deck temperature at midday is much higher than the
212 temperature on the truss. The difference in temperature between the deck and the truss is
213 larger on clear days compared to cloudier days within the same month. For the Tamar Bridge
214 the warmest monitored parts of the structure are the deck and the suspension cables, since
215 they are in direct sunlight and gain heat from solar radiation. The truss, however, is often the
216 coolest part since it is shaded by the cantilevered lanes. The supported structure is also made
217 of steel, so it loses heat stored within its thermal mass during the same day.

218 Thus ΔT_t , the difference between the temperature of the suspension cable and truss at
219 time t , was used to approximate the cloud cover levels. Use of the deck temperature was
220 considered but deck temperature occasionally fell below that of the truss and would produce
221 less reliable results than the suspension cable.

222 Solar radiation intensity rises and falls during each day, and is greater during the
 223 summer compared to winter, regardless of the cloud cover level. Both the diurnal and
 224 seasonal behaviours already feature in the Johnson-Woodward model as sinusoids (see
 225 Equations A.4, A.8 and A.12 in the Appendix). Therefore the value of ΔT_t requires
 226 modification so that it is only linked to thermal behaviour resulting from cloud cover, and
 227 removes behaviour linked to the rise and fall of the sun.

228 High-pass Butterworth filters were applied to ΔT_t data to remove sinusoidal
 229 behaviour but the resulting curves formed acute peaks at midday, when rounded curves were
 230 desirable to provide no sudden changes of cloud cover. It was found that using a simple
 231 moving average over a 21 hour interval ($r+1$) would remove the daily fluctuations to an
 232 acceptable degree:

$$\Delta T'_t = \frac{\Delta T_{t-r/2} + \dots + \Delta T_t + \dots + \Delta T_{t+r/2}}{(r+1)} \quad (7)$$

233 where $\Delta T'_t$ is the modified value of ΔT_t . The resultant peaks in the smoothed data appear at
 234 similar times as clear spells in several webcam images.

235 The final step is to normalise these values between 0 and 1 to convert them into an
 236 equivalent cloud cover factor, f_{cc} . This was also performed over a roaming interval, with the
 237 data normalised to the maximum and minimum values within a specified range. This method
 238 assumes that within the interval there is at least one instance where the sky is completely
 239 cloudless ($f_{cc} = 0$), and one instance where the sky is totally covered in cloud ($f_{cc} = 1$).

$$f_{cc,t} = \frac{\Delta T'_t - \mathbb{T}_{\min}}{\mathbb{T}_{\max} - \mathbb{T}_{\min}} \quad (8)$$

240 where $f_{cc,t}$ is the predicted cloud cover at time t , and \mathbb{T}_{\min} and \mathbb{T}_{\max} are the minimum and
 241 maximum $\Delta T'_t$ within the observed interval:

$$\mathbb{T}_{\min} = \min[\Delta T'_{t-s/2}; \dots; \Delta T'_t \dots; \Delta T'_{t+s/2}] \quad (9)$$

$$\mathbb{T}_{\max} = \max[\Delta T'_{t-s/2}; \dots; \Delta T'_t \dots; \Delta T'_{t+s/2}] \quad (10)$$

242 By testing various sizes of an interval s and comparing webcam images an interval
 243 length of 7 weeks provided acceptable values for cloud cover for the Tamar Bridge. This
 244 interval also ensures cloud cover levels are determined on a month-by-month basis, since the
 245 temperature difference is larger during the summer than winter.

246 Figure 3 presents the cloud cover predicted by the method described for the two dates
 247 seen previously. These results are compared to data monitored from Plymouth Airport that
 248 were also available for use, acquired from weather information by Wolfram Mathematica 7
 249 software. The cloud cover method produces the intended results: cloud cover factors close to
 250 1 in the January data, and low cloud cover at midday in the July data. The data collected from
 251 Plymouth Airport on the other hand do not provide an acceptable representation of the cloud
 252 cover seen in the webcam images. Apart from having just three absolute values (0.25, 0.5 and
 253 0.9) they may also be incorrect for the Tamar Bridge since the two locations are 6.9km apart,
 254 and the airport is 142m above sea level. The airport data for January 10th suggests times when
 255 there was little cloud, while the webcam images show the bridge, which is at sea level, was
 256 surrounded by fog for the whole day. Hence the developed cloud cover method was used
 257 when monitored results were available. While the levels of cloud cover may not be correct
 258 during the late evening/early morning period, these periods generally occur overnight, so
 259 would have a very limited effect on the solar radiation calculations.

260 The method described here is an innovation of the project, since it uses monitored
 261 temperature data in order to acquire a value for cloud cover that is otherwise difficult to
 262 quantify. The values determined from this method have been reasonable for further use in the
 263 solar radiation calculations. Temperature data also requires less memory storage than

264 webcam images, which allows for more opportunities of gaining further thermal information
265 by installing additional thermogauges around the structure.

266 **Applied solar radiation**

267 Using the temperatures monitored from the actual structure, approximate cloud cover levels
268 and the method described in the Appendix, estimates for the solar radiation applied to the
269 bridge were now available.

270 The radiation loads were applied to the orthotropic deck and tower faces in the FE
271 model, which were also subject to air convection and surface radiation. Due to the complex
272 arrangement of the truss, radiation effects were not applied to the underside of the bridge.
273 However on simpler structures shading could be approached in a similar way as Liu et al.
274 (2012).

275 **Application to the finite element (FE) model**

276 An FE model was developed as part of our investigations on the Tamar Bridge to assist with
277 interpretations of behaviour observed in the monitored data (Westgate and Brownjohn 2010).
278 The model was developed in ANSYS 12.1, which allows for the option of performing
279 thermal and structural analyses on the same model. A multi-physics analysis was applied to
280 combine the two sets of results: first the problem is solved via a thermal analysis to determine
281 the structure's temperature and thermal stresses, then the results were transferred as an
282 additional load for a structural analysis.

283 **FE model details**

284 The 3D FE model of the Tamar Bridge was developed from a combination of shell and line
285 elements, shown in Figure 4 (top). For structural analyses, the truss members were modelled
286 with either BEAM4 or BEAM44 three dimensional elastic beam elements. The cables and
287 hangers were modelled with LINK10 spar elements with the "tension only" option selected.

288 The plate elements that composed the deck and tower sides were modelled with SHELL63
289 elastic shell elements. The stiffness caused by friction at the bearings at the Saltash expansion
290 gap and the ends of the bridge was modelled by a series of spring elements. The properties of
291 the FE model were calibrated using modal properties (frequency and mode shape) established
292 during an ambient vibration survey (Brownjohn and Carden 2008).

293 For thermal analyses the structural element types were replaced with thermal
294 counterparts that are able to conduct heat: 3D beam elements in the model used LINK33 and
295 the plate elements used SHELL57. Convection and radiation effects were applied to plate
296 elements such as the concrete towers and the deck surface by overlaying two layers of
297 SURF151 elements, shown in Figure 4 (bottom).

298 One limitation is the inability to apply radiation to line elements such as the
299 suspension cables, since the elements in the model do not have a surface area defined. There
300 are also far too many different beam sections, each receiving different amounts of shade, to
301 perform individual radiation analyses. Instead the monitored truss temperatures were applied
302 to the nodes on the lower stringers of the truss as they directly represent its thermal response.
303 Since the suspension cable is one of the most important structural elements for determining
304 the bridge configuration, it was felt that a complete solar radiation analysis should include a
305 thermal simulation through a section of the cable. This model was made up of PLANE55
306 elements: 2D thermal solid elements with 3 or 4 nodes. Neighbouring nodes in the models,
307 such as within 1cm of the wrap or adjacent wires, were thermally coupled to transfer heat
308 between the wires and the wrap.

309 **Calibration of thermal properties**

310 The next stage was to ensure that the response from the FE model provides a good match
311 with results found during monitoring. The thermal response of the FE model was calibrated
312 to daily samples of temperature data recorded from the actual structure to adjust unknown

313 thermal properties such as the absorption, emissivity and convection coefficients of the
314 surfaces in the model. To see how the bridge responds to high and low levels of solar
315 radiation, the two dates used previously to determine cloud cover (January 10th and July 8th,
316 2010) were utilized to ensure that the peak thermal response of simulated bridge occurred at
317 the time recorded in the monitored results, with the same temperature.

318 Through a series of tests it was determined that the absorption and convection
319 coefficients were the most influential parameters governing the thermal behaviour of the
320 structure: the convection coefficient determines the time when the peak temperature occurs,
321 and the absorption coefficient affects the amplitude of the simulated temperature. By
322 adjusting each variable a solution was produced where the peaks in the simulated and
323 monitored results coincided.

324 The rise and fall of the monitored and simulated data was not a perfect match; during
325 the morning on July 8th the simulated temperatures were up to 3.8°C larger than temperatures
326 monitored from the structure. These errors were attributed to wind chill, which is not
327 accounted for within the FE model. By using the estimated cloud factors the applied radiation
328 in the FE model would be lessened during the morning and evening periods, and the error
329 reduced to within 2°C, which was considered acceptable.

330 The thermal properties of the bridge used in the FE model are presented in Table 1,
331 assuming a linear relationship with temperature between -20°C and 100°C. The adopted
332 thermal conductivity of the combined asphalt and steel deck is that of the asphalt alone, since
333 its low conductivity would determine how quickly the heat would spread. Other thermal
334 properties were adopted from the Comité Euro-International du Béton design code (Comité
335 Euro-International du Béton 1993) and the relevant British Standards (British Standards
336 Institution 2005a; b).

337 The emissivity, absorption and convection coefficients used for steel in this

338 investigation are similar to those used by Elbadry and Ghali (1983) and Branco and Mendes
339 (1993), so by comparison the properties used in this study should replicate the thermal
340 response of the material. In reality these coefficients are not likely to be constant across the
341 bridge. Certain locations on the bridge may fade since they are prone to weathering, which
342 affects their surfaces ability to absorb and emit heat. There are also irregularities within the
343 members and their coating. Since the investigation is observing the bridge's overall
344 performance, these localised distortions would provide little error to the produced results.

345 However the materials used for the bridge's construction in 1961 are subject to
346 differing manufacturing methods, and would have distorted with age. For this reason the
347 materials are not the same for members added at a later date, such as during the 2001
348 strengthening and widening exercise. This would be a likely source of error. In this
349 investigation the effect should be lessened since the newer members are typically found on
350 surface elements in the central lanes and the cantilever lanes, and were subject to surface
351 loads in the thermal analysis. These members were treated differently than older steel
352 members, which are the line elements in the truss.

353 **Diurnal and seasonal variations of thermal loading and structural response**

354 Assuming the FE model of the suspension cable and the full bridge provide an accurate
355 representation of the bridge through a transient heat analysis, they can be used to simulate the
356 bridge performance for longer periods and a variety of thermal conditions. In order to
357 determine how the bridge responds to time dependent thermal loading throughout the year,
358 sixty days of monitored performance data were chosen for a detailed study.

359 **Time series of bridge temperature**

360 Five consecutive days (10th to the 14th) were chosen for each of the 12 months in 2010 to
361 represent variations that occur seasonally, rather than just diurnally. Like the calibration tests,

362 these periods include effects of solar radiation and air convection, plus monitored truss
363 temperatures.

364 The simulated cable temperatures from the FE model in Figure 5 (top) demonstrate a
365 good fit with the monitored results with occasional anomalies. There are errors between the
366 simulated and monitored results that tend to occur around midday during October, when the
367 monitored cable temperatures are much higher than the simulated temperatures. Observations
368 at night provide a close match, which indicates that the simulated solar radiation was too high
369 for this period. Overall the median error from the deck temperatures is 0.59°C and the
370 monitored and simulated data sets have a correlation coefficient of 0.968, which the
371 researchers view as a satisfactory match.

372 Compared to the cable results, Figure 5 (middle) also demonstrates a good agreement
373 between the results monitored from the bridge and the simulated temperatures from the FE
374 model. Errors generally occur when the peak daily temperatures do not match the monitored
375 results at noon, which appears to be the same error as seen in the cable temperatures. It is also
376 possible that monitored results may be lower than predicted due to wet conditions, when
377 surface water absorbs heat.

378 Simulated temperature time series for the southern face of Plymouth tower in Figure 5
379 (bottom) show that their peak temperature occurs between 2 to 4 hours after the peak
380 temperature of the deck. The tower continues to lose heat into the following morning, since
381 the concrete of the towers loses heat to convection and heat radiation more slowly compared
382 to the steel elements. While there is no monitored data available, since there are no
383 thermogauges currently attached to the towers, the FE simulated behaviour is similar to the
384 monitored thermal response of the Zhang-Jiang Bay Bridge's concrete towers (Cao et al.
385 2010), for which the same conclusion was drawn about the material properties.

386 **Time series of quasi-static displacement of the suspended structure**

387 Figure 6 presents the structural displacement time series for 10 days of observed data: 5 days
388 taken during July and the remaining 5 during October. The time series compare the results
389 predicted from the FE analysis at midspan (CG062 in Figure 1) to the monitored results. Both
390 sets of data show larger movements of the deck when there are larger variations in deck
391 temperature, as expected. For the most part the simulated time series overlap the monitored
392 results, providing a correlation coefficient of 0.970 for expansion, and 0.958 for vertical
393 deflection. The FE results tend to overestimate the peak deflections at midday: on July 11th
394 there is up to 64mm of error between the vertical deflection data sets. This is partly because
395 of errors produced in the temperature results. Additionally these overestimates occur
396 whenever the temperature gradient through the suspended is large. This implies that low truss
397 temperatures require more influence on the simulated thermal movements to better represent
398 the behaviour seen in the monitored results. The thermal expansion relating to the truss
399 temperature is further discussed in a later section of this paper.

400 The sway of the tower tops was also considered to see if their structural performance
401 coincided with their thermal performance (in Figure 5 bottom) and to see whether the time of
402 peak sway is 4 hours after the peak deck expansion shown previously in Figure 6. However
403 the results in Figure 7 show little resemblance in the behaviour between the two towers,
404 suggesting that other variables are involved. For instance, the sway of the Plymouth tower
405 (top) in both the monitored and FE results moves west during the morning. The sway
406 displacements typically peak at midday like the deck displacements, rather than mid-
407 afternoon like the tower temperature time series. This phenomenon is linked to the
408 longitudinal movement of the suspended structure towards the expansion gap at the Saltash
409 tower. As the deck moves outwards, the stay cables pull the Plymouth tower towards
410 midspan.

411 The time series of the simulated Saltash tower deflections (bottom) move in the
412 opposite direction of the Plymouth tower. The displacement at the Saltash tower's top are not
413 as large as at Plymouth, so the Saltash tower is not so affected by the attached stay cables'
414 tensions. The behaviour of the tower also shows little association with the deck
415 displacements; the mainly irregular line formed from the data suggests a dynamic influence
416 such as traffic and wind.

417 To summarise, the qualitative observations in the temperature and structural time
418 series suggests behaviours that were either directly linked or were delayed by a few hours.
419 The following sections detail the systematic examinations on the data to identify the
420 collective mechanisms that cause this behaviour, as well as their influence on the
421 relationships.

422 **Relationships found within the bridge behaviour**

423 **Relationship of expansion with temperature**

424 In order to see how the solar intensity affects the quasi-static configuration of the bridge,
425 Figure 8 plots the FE simulated midspan deflections against the temperature of the deck,
426 suspension cable and the truss. The samples are split into two groups, depending on whether
427 the applied solar intensity was below $50\text{W}/\text{m}^2$, which is at night or during winter, or above.

428 For periods when the solar intensity is less than $50\text{W}/\text{m}^2$ (top left of Figure 8) the
429 expansion of the bridge deck at midspan has a linear relationship with temperature, since the
430 temperature differential across the bridge section is small. For data where the applied solar
431 radiation exceeds $50\text{W}/\text{m}^2$ (top right) the relationship for all three temperature parameters
432 with the deck expansion turns nonlinear. The deck expands further than the truss, and if the
433 cables were not present the supported structure would curve upwards. At this level of solar
434 radiation the temperature differential between the deck and the truss is more pronounced and

435 it is more evident that the thermal expansion is a product of two or more parameters. Similar
436 behaviour is observed in the vertical deflections at the mid-span (bottom), except the
437 relationship of the suspended structure sag to the suspension cables' temperature appears to
438 be highly linear.

439 Analysts may consider adopting an effective temperature as an average of the deck,
440 truss and suspension cable temperatures, but this assumes that all three are equally important
441 for longitudinal and vertical movements. For structural systems like the Tamar Bridge this
442 may not be the case. While the orthotropic deck is wide and experiences large fluctuations in
443 diurnal temperature, the stiffness of the suspended structure is mainly provided by the truss,
444 which is warmed by the air underneath the deck. Likewise the suspension cable provides
445 more vertical support to the structure than the deck system.

446 Considering the various nonlinearities appearing in the data, it seems that
447 mathematical models should attempt to account for all three thermal parameters, revealing
448 their relative influence on bridge response through their coefficients. One approach is
449 response surface modelling, which is similar to regression analyses, by using the least squares
450 method to weight polynomial coefficients linking input parameters to a specific single output.
451 In this case the inputs are the temperature data, and the output is a thermal displacement. This
452 method is straightforward and provides direct interpretation of the physical behaviour of the
453 bridge. Response surface models have been used on the Tamar Bridge before by Cross et al.
454 (2013) to associate a variety of environmental and operational factors with the response of the
455 first mode of vibration.

456 Fitting a surface to the 60 days of data with longitudinal displacements as the output
457 generates coefficients shown in Table 2. The coefficients indicate that the longitudinal
458 expansion of the supported structure is more dependent on temperature of the deck and the
459 truss, while other inputs such as the suspension cable temperature have a smaller effect. For

460 the vertical deflection, the largest coefficient is associated with the suspension cable
461 temperature. This indicates the rise of the suspended structure is mostly dependent on the
462 thermal response of the suspension cable rather than its own temperature.

463 Comparing the coefficients between the monitored and simulated data sets, the model
464 for monitored results imply the truss temperature accounts for almost a third of the bridge's
465 expansion, while the thermal response determined by the FE model is mostly determined by
466 the temperature of the deck. Similarly the vertical deflections in the monitored results show
467 more dependency on the truss temperature than the simulated deflections. This was
468 observable in the time series shown previously in Figure 6, where the thermal deflections in
469 simulated results are over estimates of the monitored results. This implies that the FE model
470 needs to be updated so that the truss should have slightly more bearing on the simulated
471 deflections. Modifications to the FE model did not provide a considerable improvement of
472 the results but after several attempts it would seem that either the axial stiffness of the truss
473 may be larger than expected or the connections between the deck and the truss are too stiff. It
474 has also been noted that response surface models based on monitored data differ on a month
475 by month basis, so it is possible that there are changes to the actual structure's configuration
476 due to seasonal behaviour and a single model is insufficient.

477

478 **Effect of cable temperature on Saltash and Plymouth tower sway**

479 Figure 9 plots the monitored and FE simulated tower displacements against the suspension
480 cable temperature to check whether their different behaviour is linked to the thermal response
481 of the structure. The monitored deflections of the Saltash tower (top left) do not show a clear
482 linear relationship with the cable temperature due to the irregularity of the Saltash tower
483 deflection time series (Figure 7). The FE results (bottom left) of the Saltash tower show a
484 shallow linear trend with temperature, compared to the trend for the Plymouth tower (top

485 right) which is steeper. As stated previously diurnal Saltash tower sway is mostly
486 independent of the bridge's thermal response, reacting to wind speeds and vehicle loads
487 instead. However if the points are shading-coded to the time of day they occur a line of black
488 dots appears in the monitored results, which are designated for samples collected between
489 20:00 and 04:00. This shows that temperature induced deflections on the Saltash tower can be
490 observed from seasonal variations, while during the day other factors govern.

491 For the Plymouth tower (top right) the linear relationship between temperature and
492 tower sway shows that an increase in cable temperature goes with the Plymouth tower
493 deflecting towards the mid-span. There is some phase difference in the relationship, causing
494 otherwise linear trends to open slightly to form elliptic loops. The underlying linearity
495 indicates that it is mostly the thermal response of the suspended structure and the cables that
496 governs the Plymouth tower sway, rather than the delayed thermal response of the tower.

497 Points in the monitored results for both towers do not fall perfectly on a single line,
498 unlike the FE results (Figure 9 bottom). The shading-coded points in the top plots
499 demonstrate that the monitored data are made up of several offset 'bands'. The offsets are not
500 due to extended loading such as traffic jams as these cause relatively small deflections, no
501 more than 4mm. A line in the plots with the monitored results show where samples collected
502 from May 2010 lie. These have a linear relationship but deflections are lower than at other
503 times during the year. This shows that the bands in the plots are seasonal deviations of the
504 monitored displacements caused by the towers reconfiguring over the course of the year, in
505 response to changing tensions in the suspension and stay cables. This may be caused by the
506 position of the sun, since during the summer the sun rises over the top of the bridge, rather
507 than to its south side, and the structural members would be warmed from three of its sides.
508 However, this is only a hypothesis, since the north-south position could not be included in the
509 adopted method for simulating solar radiation.

510

511 **Summary and conclusions**

512 This investigation presents monitored thermal induced behaviour observed on the Tamar
513 Bridge taken from five days in each month for a whole year. The mechanisms that cause this
514 behaviour were explored by applying simulated solar radiation effects to a complete FE
515 model of the bridge.

516 The following conclusions have been drawn from this investigation:

- 517 • Cloud cover information can be reasonably approximated from the relative temperature
518 difference through the deck over a period of a month.
- 519 • On most of the examined days, the temperature of the deck was first to reach its peak
520 compared to the rest of the structure, which is due to the asphalt layer and the orthotropic
521 decks slenderness. The suspension cable peaked an hour later, while the concrete towers
522 reached their maximum temperature 4 hours after the deck's maximum temperature, since
523 concrete is more capable of retaining than steel.
- 524 • The thermal expansion of the suspended structure is linked to the combined temperature of
525 the deck and the truss, while its sag is dependent on the thermal elongation of the
526 suspension cable.
- 527 • The behaviour of the Saltash tower was mostly unrelated to the diurnal thermal behaviour
528 of the bridge, since it is located near the main span expansion gap. However, a seasonal
529 thermal response was observed if only early morning samples were considered.
- 530 • The sway of the Plymouth tower was linked to the thermal expansion of the deck, which
531 pulled it towards the bridge midspan as the bridge warmed up.

532 **Acknowledgements**

533 Thanks to David List and Richard Cole of Tamar Bridge for their enduring support for the

534 research. The research was funded by EU FP7 project IRIS and EPSRC grants EP/F035403/1
535 and EP/G0611301/1.

536 **Appendix**

537 **A.1 Daily values**

538 The majority of the steps shown here have been duplicated from a paper by Rivington et al.
539 (2005).

540 Total daily irradiance, J_0 is given by

$$DJ_0 = SJ_{0,s} + DJ_{0,d} \quad (\text{A.1})$$

541 where D is the day length, S the sunshine duration, $J_{0,s}$ the direct beam component and
542 $J_{0,d}$ the diffuse component. The day length in hours is calculated by

$$D = \frac{24}{\pi} \cos^{-1}(-\tan \lambda \tan \delta) \quad (\text{A.2})$$

543 where λ is the latitude of the location and δ the solar declination, both measured in radians.
544 The solar declination for a day in a year may be found by

$$\delta = -0.4084 \cos\left(2\pi \frac{d+10}{365}\right) \quad (\text{A.3})$$

545 where d is the day of the Year (e.g. $d = 1$ for January 1st).

546 The direct beam component is given by

$$J_{0,s} = 1367 \frac{2p}{\pi} \left(\tau^{1/\sin \varnothing_0}\right) \sin \varnothing_0 \quad (\text{A.4})$$

547 where p is the fraction of radiation in full spectrum sunlight (1 has been used, for simplicity),
548 1367 is the solar constant (in W/m^2), τ is the atmospheric transmissivity and \varnothing_0 is the solar
549 elevation at noon, in radians: $\sin \varnothing_0$ may be found via

$$\sin \varnothing_0 = \sin \lambda \sin \delta + \cos \lambda \cos \delta \quad (\text{A.5})$$

550 Atmospheric transmissivity, τ , was calculated as a function of the elevation (ν) and
 551 range of diurnal air temperature values on site (ΔT), as provided by Coops et al. (2000),
 552 following a similar model developed by Thornton and Running (1999).

$$\tau = (0.65 + 0.008\nu) \cdot [1 - \exp(-B \cdot \Delta T^{1.5})] \quad (\text{A.6})$$

553 where ν is 43.2m for Tamar Bridge, and

$$B = 0.031 + 0.201 \exp(-0.185 \cdot \Delta T) \quad (\text{A.7})$$

554 This is an alternative to the formula used by Woodward et al. (2001), where
 555 atmospheric transmissivity was a function of the day of the year. This was not adopted since
 556 the range of monitored air temperatures at Plymouth was similar for the whole observed year,
 557 probably due to atypical seasonal cloud cover, and as a result atmospheric transmissivity is
 558 affected. Baigorria et al. (2004) has shown that transmissivity models relating to the air
 559 temperature demonstrate more reliable results for the Andes compared to models that are
 560 dependent on time.

561 The diffuse portion of total irradiance $J_{0,d}$ can be calculated by

$$J_{0,d} = J_{0,p} (f_{blue} \cdot (1 - f_{cc}) + f_{cloud} \cdot f_{cc}) \quad (\text{A.8})$$

562 where f_c is the mean daily cloud cover, which is assumed to be $f_c = 1 - (S/h)$, being a
 563 dimensionless value between 0 (no cloud cover) and 1 (complete cloud cover).

564 $J_{0,p}$ is the potential total clear sky mean daily irradiance, which is calculated by

$$J_{0,p} = 1367 \frac{P}{\pi} (1 + \tau^{1/\sin \varnothing_0}) \sin \varnothing_0 \quad (\text{A.9})$$

565 The values of f_{blue} and f_{cloud} are the relative radiation intensities under blue sky and

566 cloudy conditions, respectively.

$$f_{blue} = \frac{1 - \tau^{1/\sin\varnothing_0}}{1 + \tau^{1/\sin\varnothing_0}} \quad (\text{A.10})$$

$$f_{cloud} = F \cdot f_{blue} \quad (\text{A.11})$$

567 The parameter F varies depending on the site. For the UK the mean yearly value of F
568 varies between 0.69 and 0.87. For the purposes of this study a value of 0.884 was taken,
569 which is the value found at Aberporth; the closest available site being 195km away from
570 Plymouth (Miller et al. 2008).

571 **A.2 Half-hourly values**

572 Following the identification of total daily irradiance, the next step is to identify the amount of
573 radiation upon the bridge in half-hourly steps. The daily course of the sun takes a cosine
574 pattern; providing 0 radiation between dusk and the dawn of the following day, and reaches
575 its peak at solar noon. Thus the hourly dependent formula for solar radiation, J_t , taken from
576 Chen et al. (1999), is

$$J_t = J_0 \cos\left(\frac{\theta - \theta_0}{\pi/2 - \theta_0} \cdot \frac{\pi}{2}\right) \quad (\text{A.12})$$

577 where θ is the solar zenith angle and θ_0 is the solar zenith angle at solar noon, which is not
578 necessarily at 12:00pm. This formula is only applicable when $\theta < \pi/2$, otherwise the sun
579 will be beyond the horizon; hence no sunlight!

580 **A.3 Factor for inclined surfaces**

581 If the surface is inclined, such as on the towers, it is likely that it will be within its own shade
582 when the sun is on its opposite side. Thus the direct beam component in Equation (A.4) has
583 to be adjusted (Sellers et al. 1997; Wang et al. 2002):

$$J_{0,s,i} = f_i \cdot J_{0,s} \quad (\text{A.13})$$

584 where f_i is the direct beam correction factor, which is limited to values between 0 and 1.

585 This value is dependent on the angle of the slope and the solar zenith angle θ :

$$f_i = \frac{\cos \theta_i}{\cos \theta} \quad (\text{A.14})$$

586 where θ_i is the angle between the solar zenith angle to the slope normal, which is determined

587 from the inclination from the horizontal for the slope β , the aspect of the face γ (North =

588 zero, East = 90°), the solar zenith angle and the solar azimuth ψ (North = zero, East = 90°).

$$\cos \theta_i = \cos \beta \cos \theta + \sin \beta \sin \theta \cos(\psi - \gamma) \quad (\text{A.15})$$

589

590 **References**

591 Baigorria, G. A., Villegas, E. B., Trebejo, I., Carlos, J. F., and Quiroz, R. (2004).

592 “Atmospheric transmissivity: distribution and empirical estimation around the central
593 Andes.” *International Journal of Climatology*, 24(9), 1121–1136.

594 Branco, F. A., and Mendes, P. A. (1993). “Thermal actions for concrete bridge design.”

595 *Journal of Structural Engineering*, 119(8), 2313–2331.

596 British Standards Institution. (2005a). *Eurocode 2. Design of concrete structures. General
597 rules. Structural fire design*. United Kingdom, 1–100.

598 British Standards Institution. (2005b). *Eurocode 3. Design of steel structures. General rules.
599 Structural fire design*. United Kingdom, 1–84.

600 Brownjohn, J. M. W., and Carden, P. (2008). “Real-time operation modal analysis of Tamar
601 Bridge.” *IMAC-XXVI: Conference & Exposition on Structural Dynamics*, Orlando,
602 Florida, USA, 1–8.

603 Cao, Y., Yim, J., Yang, Z., and Wang, M. L. (2010). "Temperature effects on cable stayed
604 bridge using health monitoring system: a case study." *Structural Health Monitoring*,
605 10(5), 523–537.

606 Chen, J. M., Liu, J., Cihlar, J., and Goulden, M. L. (1999). "Daily canopy photosynthesis
607 model through temporal and spatial scaling for remote sensing applications." *Ecological*
608 *modelling*, Elsevier, 124(2-3), 99–119.

609 Churchward, A., and Sokal, Y. J. (1981). "Prediction of Temperatures in Concrete Bridges."
610 *Journal of the Structural Division*, 107(11), 2163–2176.

611 Comité Euro-International du Béton. (1993). *CEB-FIP Model Code 1990: Design Code*.
612 Thomas Telford Limited, 61–66.

613 Coops, N. C., Waring, R. H., and Moncrieff, J. B. (2000). "Estimating mean monthly incident
614 solar radiation on horizontal and inclined slopes from mean monthly temperatures
615 extremes." *International Journal of Biometeorology*, Springer Berlin / Heidelberg,
616 44(4), 204–211.

617 Cross, E., Koo, K. Y., Brownjohn, J. M. W., and Worden, K. (2013). "Long-term monitoring
618 and data analysis of the Tamar Bridge." *Mechanical Systems and Signal Processing*,
619 35(1-2), 16–34.

620 Cross, E., Worden, K., Koo, K.-Y., and Brownjohn, J. M. W. (2011). "Co-integration and
621 SHM of bridges." *8th International Workshop on Structural Health Monitoring*,
622 Stanford, California.

623 Ding, Y.-L., and Li, A. (2011a). "Temperature-induced variations of measured modal
624 frequencies of steel box girder for a long-span suspension bridge." *International Journal*
625 *of Steel Structures*, Korean Society of Steel Construction, co-published with Springer,
626 11(2), 145–155.

627 Ding, Y.-L., and Li, A. (2011b). "Assessment of bridge expansion joints using long-term
628 displacement measurement under changing environmental conditions." *Frontiers of*
629 *Architecture and Civil Engineering in China*, Higher Education Press, co-published with
630 Springer-Verlag GmbH, 5(3), 374–380.

631 Elbadry, M. M., and Ghali, A. (1983). "Temperature variations in concrete Bridges." *Journal*
632 *of Structural Engineering*, 109(10), 2355–2374.

633 Hirst, M. J. S. (1984). "Thermal loading of concrete bridges." *Canadian Journal of Civil*
634 *Engineering*, NRC Research Press Ottawa, Canada, 11(3), 423–429.

635 Ho, D., and Liu, C.-H. (1989). "Extreme Thermal Loadings in Highway Bridges." *Journal of*
636 *Structural Engineering*, 115(7), 1681–1696.

637 Johnson, I. R., Riha, S. J., and Wilks, D. S. (1995). "Modelling daily net canopy
638 photosynthesis and its adaptation to irradiance and atmospheric CO₂ concentration."
639 *Agricultural Systems*, Elsevier, 50(1), 1–35.

640 Koo, K. Y., Brownjohn, J. M. W., List, D. I., and Cole, R. (2012). "Structural health
641 monitoring of the Tamar suspension bridge." *Structural Control and Health Monitoring*,
642 20(4), 609–625.

643 Koo, K.-Y., de Battista, N., and Brownjohn, J. M. W. (2011). "SHM data management
644 system using MySQL database with MATLAB and Web interfaces." *Proceedings of the*
645 *5th International Conference on Structural Health Monitoring of Intelligent*
646 *Infrastructure (SHMII-5)*, Cancun, Mexico, 1–9.

647 Koo, K.-Y., Brownjohn, J. M. W., List, D., Cole, R., and Wood, T. (2010). "Innovative
648 Structural Health Monitoring for Tamar Suspension Bridge by Automated Total
649 Positioning System." *Proceedings of the 7th International Conference on Bridge*
650 *Maintenance, Safety and Management (IABMAS)*, 1–8.

651 Liu, C., DeWolf, J. T., and Kim, J.-H. (2009). "Development of a baseline for structural
652 health monitoring for a curved post-tensioned concrete box-girder bridge." *Engineering*
653 *Structures*, 31(12), 3107–3115.

654 Liu, H., Chen, Z., and Zhou, T. (2012). "Theoretical and experimental study on the
655 temperature distribution of H-shaped steel members under solar radiation." *Applied*
656 *Thermal Engineering*, 37, 329–335.

657 Miao, C.-Q., Chen, L., and Feng, Z.-X. (2011). "Research on correlation of modal frequency
658 of long-span bridge structures and environmental temperature." *2011 International*
659 *Conference on Multimedia Technology*, IEEE, Hangzhou, 1175–1179.

660 Miller, D. G., Rivington, M., Matthews, K. B., Buchan, K., and Bellocchi, G. (2008).
661 "Testing the spatial applicability of the Johnson-Woodward method for estimating solar
662 radiation from sunshine duration data." *Agricultural and forest meteorology*, Elsevier,
663 148(3), 466–480.

664 Minhoto, M. J. C., Pais, J. C., Pereira, P. A. A., and Picado-Santos, L. G. (2005). "Predicting
665 asphalt pavement temperature with a three-dimensional Finite Element method."
666 *Transportation Research Record: Journal of the Transportation Research Board*, 1919,
667 96–110.

668 Moorty, S., and Roeder, C. W. (1992). "Temperature-Dependent Bridge Movements."
669 *Journal of Structural Engineering*, 118(4), 1090–1105.

670 Ni, Y. Q., Hua, X. G., Wong, K.-Y., and Ko, J. M. (2007). "Assessment of Bridge Expansion
671 Joints Using Long-Term Displacement and Temperature Measurement." *Journal of*
672 *Performance of Constructed Facilities*, 21(2), 143–151.

673 Peeters, B., and De Roeck, G. (2001). "One-year monitoring of the Z24-Bridge:
674 environmental effects versus damage events." *Earthquake Engineering & Structural*
675 *Dynamics*, 30(2), 149–171.

676 Rivington, M., Bellocchi, G., Matthews, K. B., and Buchan, K. (2005). "Evaluation of three
677 model estimations of solar radiation at 24 UK stations." *Agricultural and forest*
678 *meteorology*, Elsevier, 132(3-4), 228–243.

679 Sellers, P. J., Heiser, M. D., Hall, F. G., Verma, S. B., Desjardins, R. L., Schuepp, P. M., and
680 MacPherson, J. I. (1997). "The impact of using area-averaged land surface properties—
681 topography, vegetation condition, soil wetness—in calculations of intermediate scale
682 (approximately 10 km²) surface-atmosphere heat and moisture fluxes." *Journal of*
683 *Hydrology*, 190(3-4), 269–301.

684 Sohn, H. (2007). "Effects of environmental and operational variability on structural health
685 monitoring." *Philosophical transactions. Series A, Mathematical, physical, and*
686 *engineering sciences*, 365(1851), 539–60.

687 Thornton, P. E., and Running, S. W. (1999). "An improved algorithm for estimating incident
688 daily solar radiation from measurements of temperature, humidity, and precipitation."
689 *Agricultural and Forest Meteorology*, 93(4), 211–228.

690 Tong, M., Tham, L. G., and Au, F. T. K. (2002). "Extreme thermal loading on steel bridges in
691 tropical region." *Journal of Bridge Engineering*, 7(6), 357–366.

692 Tong, M., Tham, L. G., Au, F. T. K., and Lee, P. K. K. (2001). "Numerical modelling for
693 temperature distribution in steel bridges." *Computers and Structures*, Elsevier, 79(6),
694 583–593.

695 Wang, S., Chen, W., and Cihlar, J. (2002). "New calculation methods of diurnal distribution
696 of solar radiation and its interception by canopy over complex terrain." *Ecological*
697 *Modelling*, 155(2-3), 191–204.

698 Westgate, R. J., and Brownjohn, J. M. W. (2010). "Development of a Tamar Bridge Finite
699 Element Model." *Proceedings of IMAC XXVIII*, Springer New York, Jacksonville, FL,
700 USA.

701 Woodward, S. J. R., Barker, D. J., and Zyskowski, R. F. (2001). "A practical model for
702 predicting soil water deficit in New Zealand pastures." *New Zealand Journal of*
703 *Agricultural Research*, Taylor & Francis, 44(1), 91–109.

704 Xia, Y., Chen, B., Zhou, X., and Xu, Y. L. (2013). "Field monitoring and numerical analysis
705 of Tsing Ma Suspension Bridge temperature behavior." *Structural Control and Health*
706 *Monitoring*, 20(4), 560–575.

707 Xia, Y., Xu, Y. L., Wei, Z. L., Zhu, H. P., and Zhou, X. Q. (2011). "Variation of structural
708 vibration characteristics versus non-uniform temperature distribution." *Engineering*
709 *Structures*, 33, 146–153.

710 Xu, Y. L., Chen, B., Ng, C. L., Wong, K.-Y., and Chan, W. Y. (2010). "Monitoring
711 temperature effect on a long suspension bridge." *Structural Control and Health*
712 *Monitoring*, 17, 632–652.

713 Zhou, H. F., Ni, Y. Q., and Ko, J. M. (2010). "Constructing input to neural networks for
714 modeling temperature-caused modal variability: Mean temperatures, effective
715 temperatures, and principal components of temperatures." *Engineering Structures*,
716 32(6), 1747–1759.

717

Table 1: Typical heat transfer properties

Property	Suspension cable		Bridge deck		Towers	
	@ -20°C	@ 100°C	@ -20°C	@ 100°C	@ -20°C	@ 100°C
<i>k</i> , thermal conductivity (W/m°C)	54.7	50.7		2.5	1.71	1.50
<i>c</i> , heat capacity (J/kg°C)	416	488		680		900
<i>h</i> , convection coefficient (W/m ² C)		18.5		26		25
ε , emissivity coefficient		0.8		0.9		0.7
α , absorption coefficient		0.75		0.9		0.65

Table 2: Coefficients determined from response surface models predicting bridge displacements at midspan.

	Temperature variable	Coefficient with FE simulated data	with monitored data
Longitudinal	Deck	+3.00mm/°C	+2.05mm/°C
	Truss	+0.26mm/°C	+1.33mm/°C
Vertical	Deck	-1.53mm/°C	-1.12mm/°C
	Cable	-10.80mm/°C	-5.51mm/°C
	Truss	+0.44mm/°C	-3.45mm/°C

Figure 1
[Click here to download high resolution image](#)

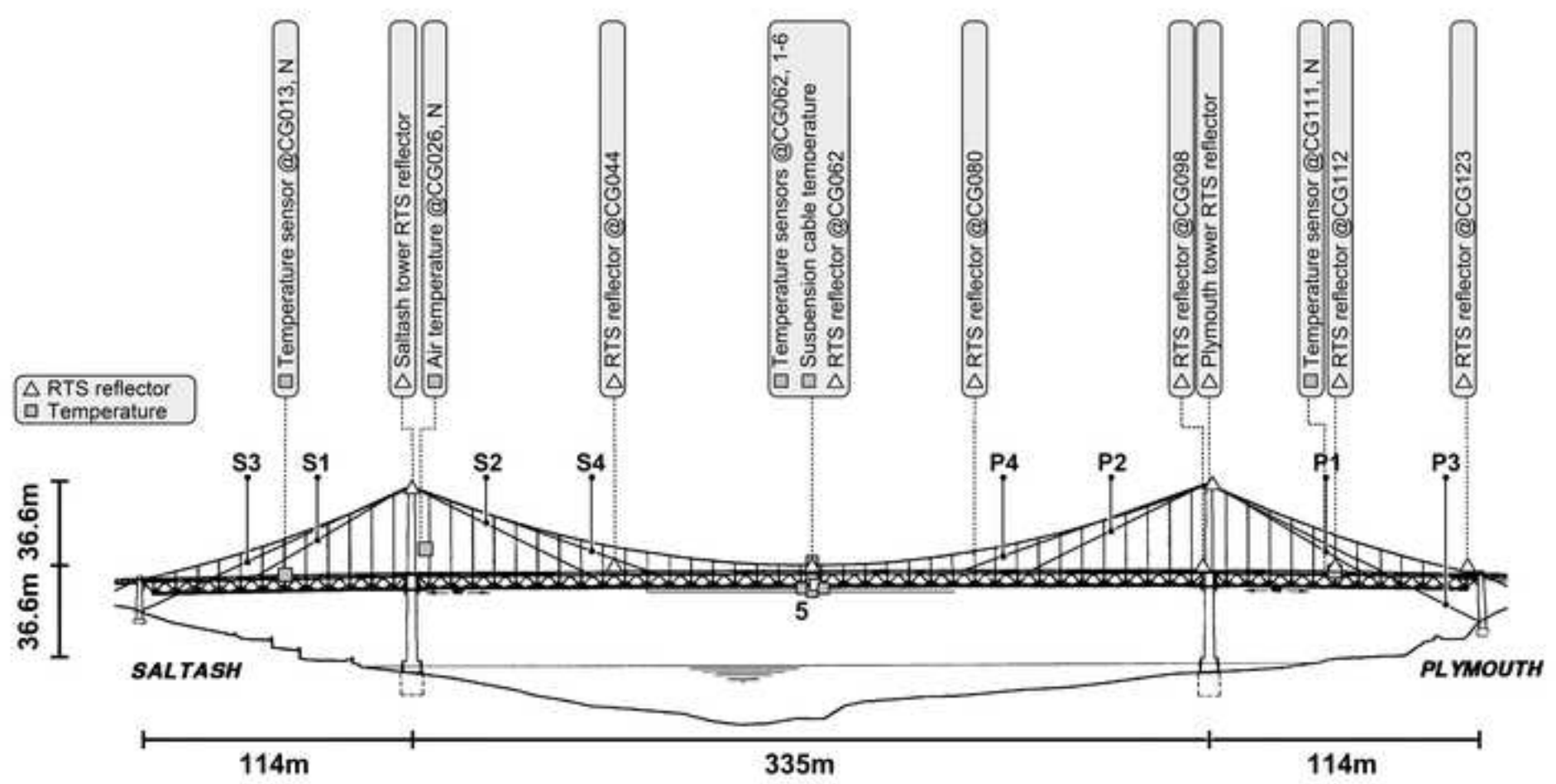


Figure 2

[Click here to download Figure: f_2b.eps](#)

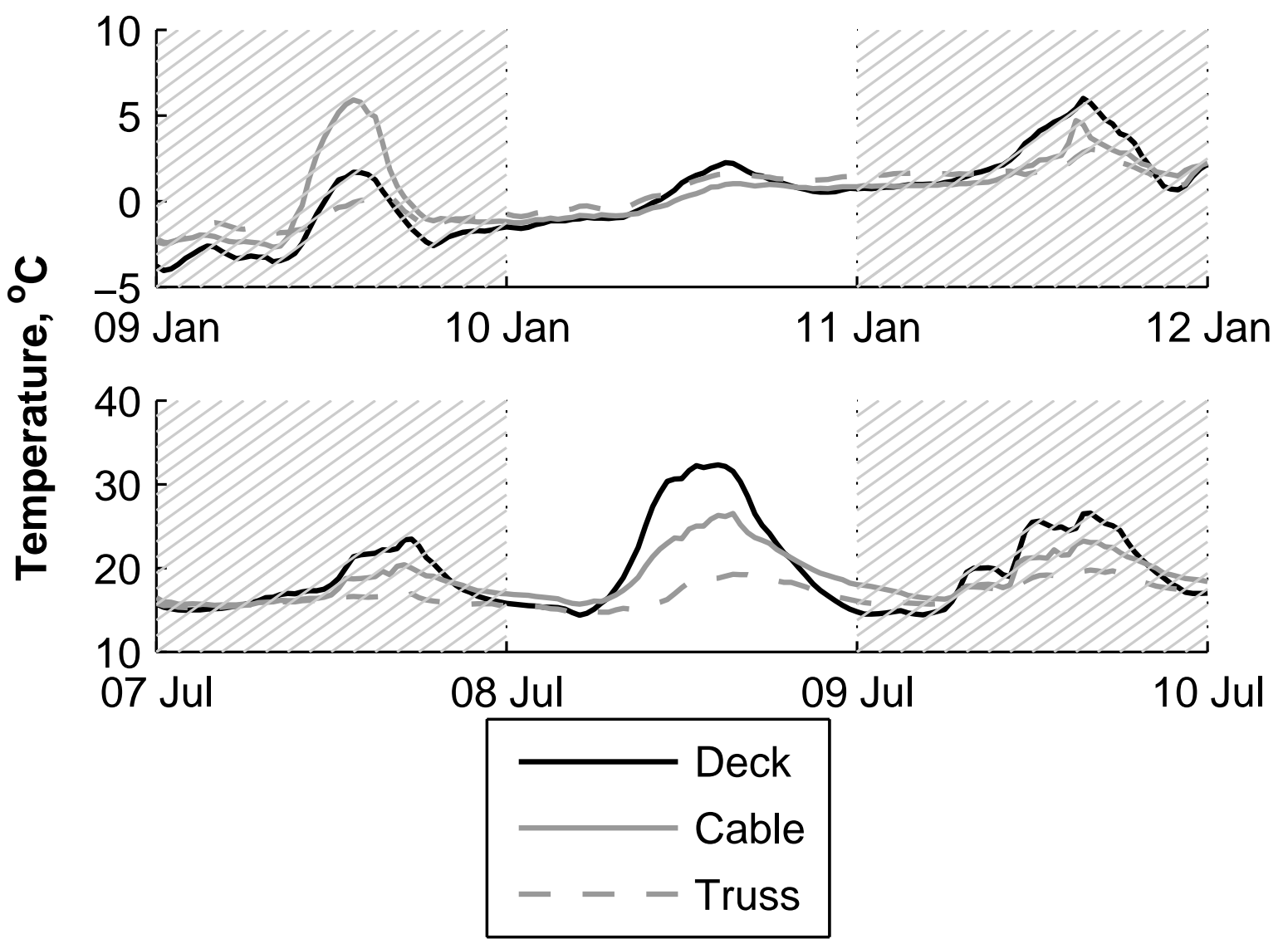


Figure 3
[Click here to download Figure: f_3b.eps](#)

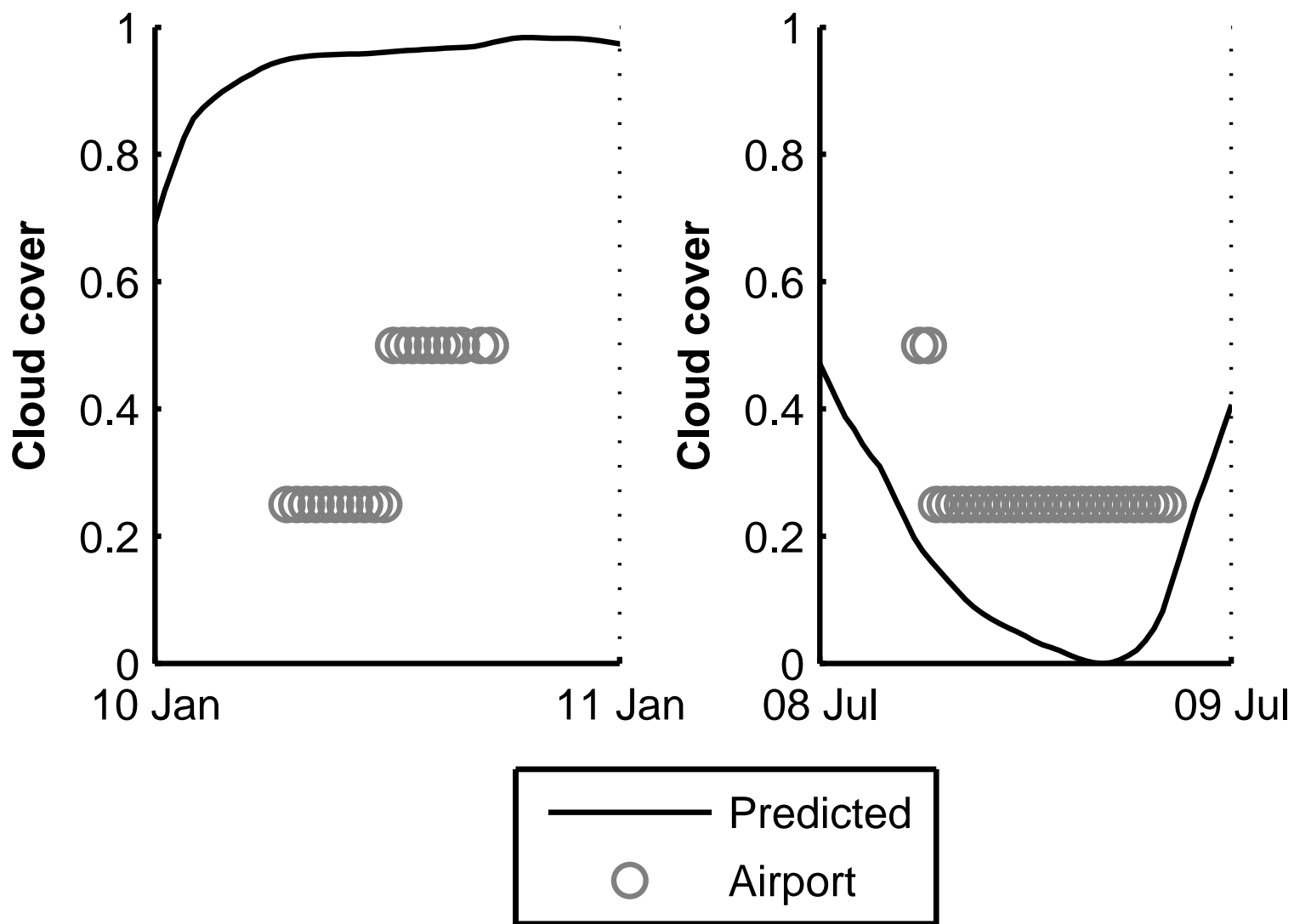


Figure 4
[Click here to download high resolution image](#)

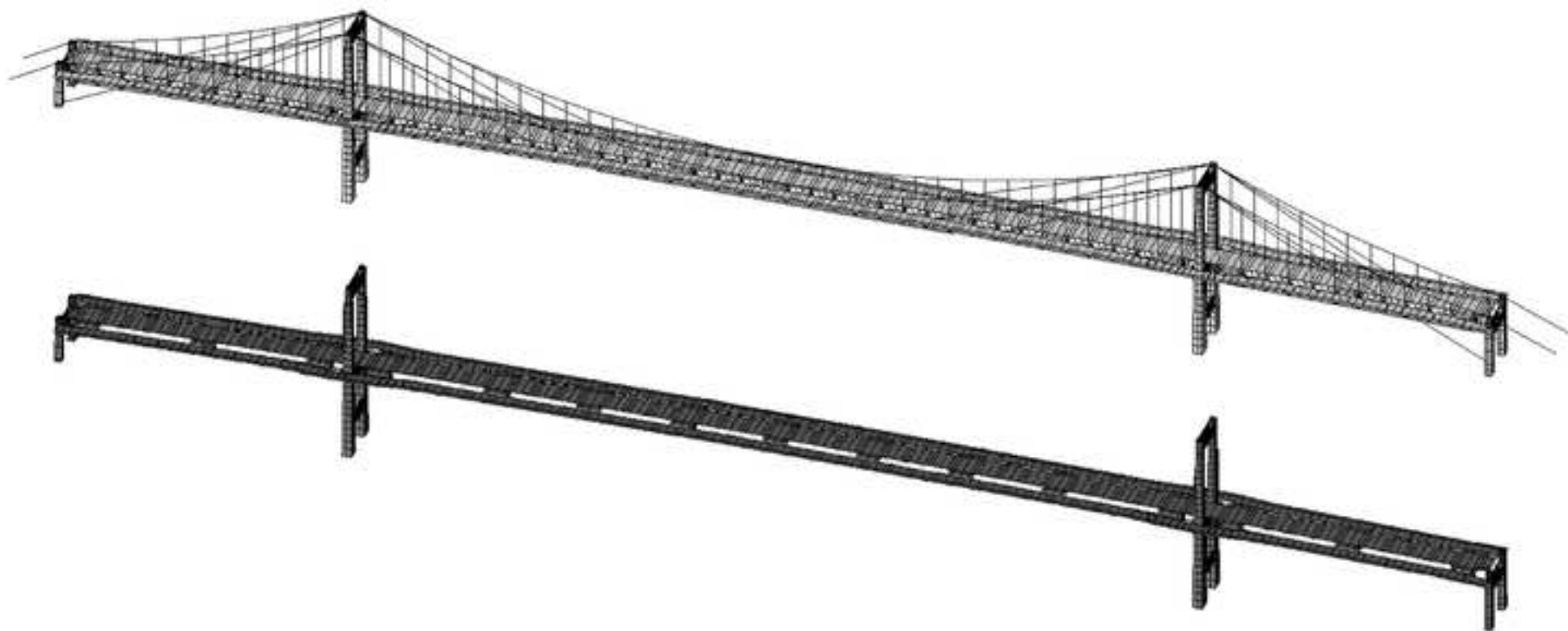
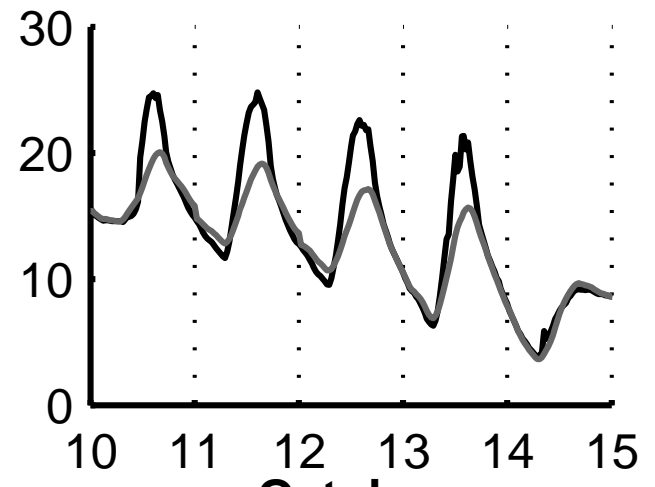
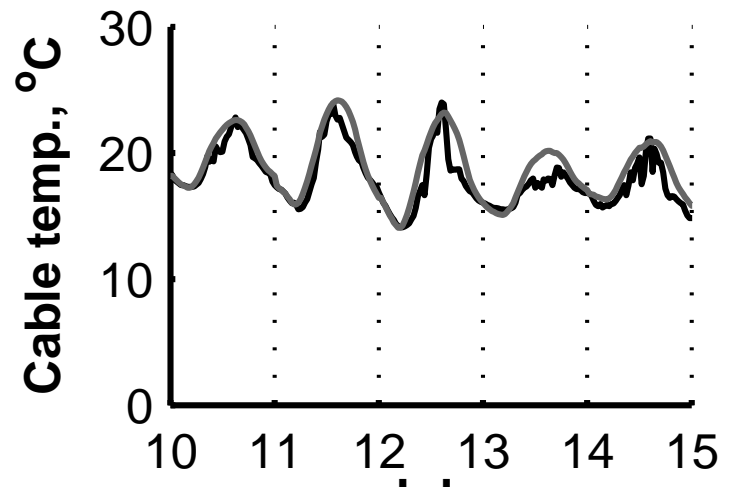


Figure 5

[Click here to download Figure: f_5b.eps](#)

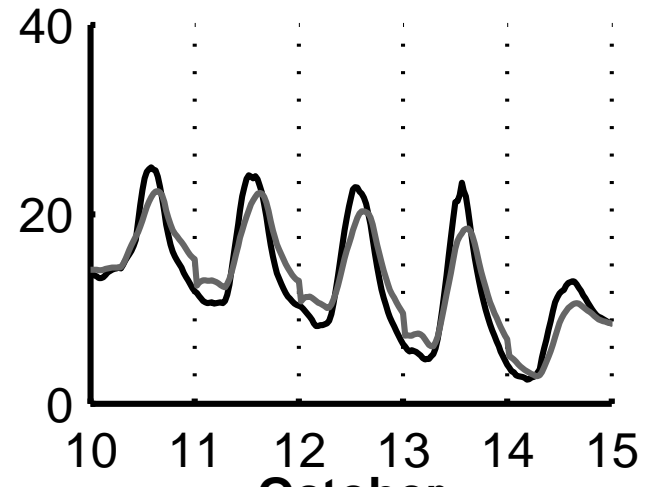
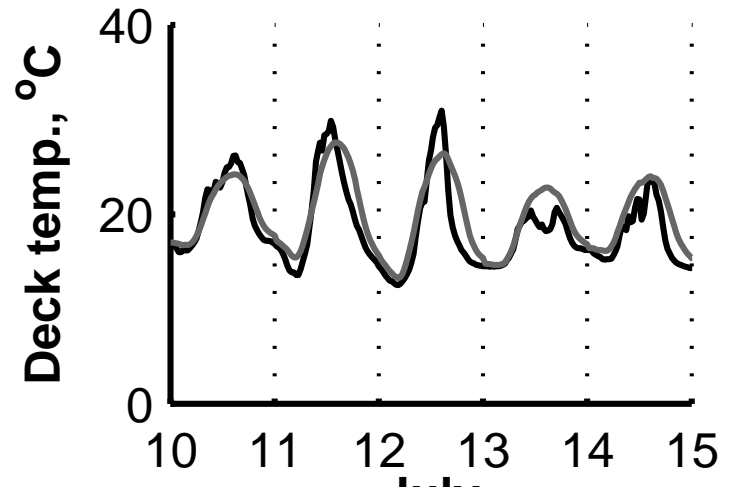
July

October



July

October



July

October

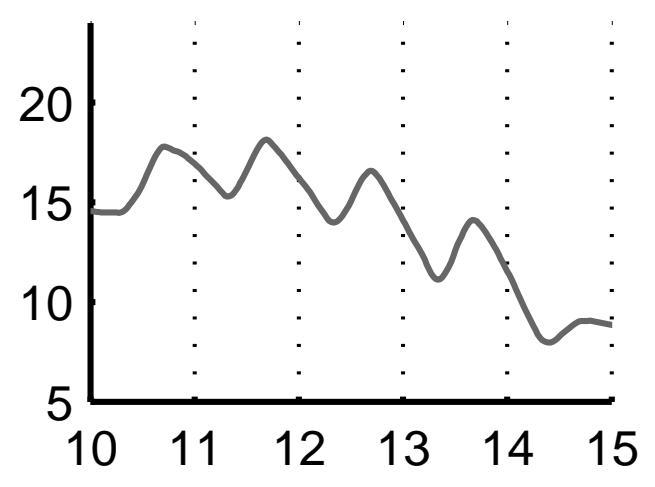
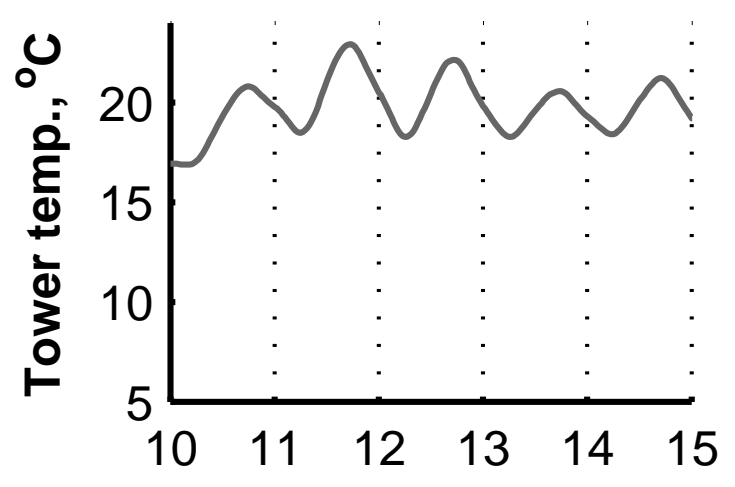


Figure 6

[Click here to download Figure: f_6b.eps](#)

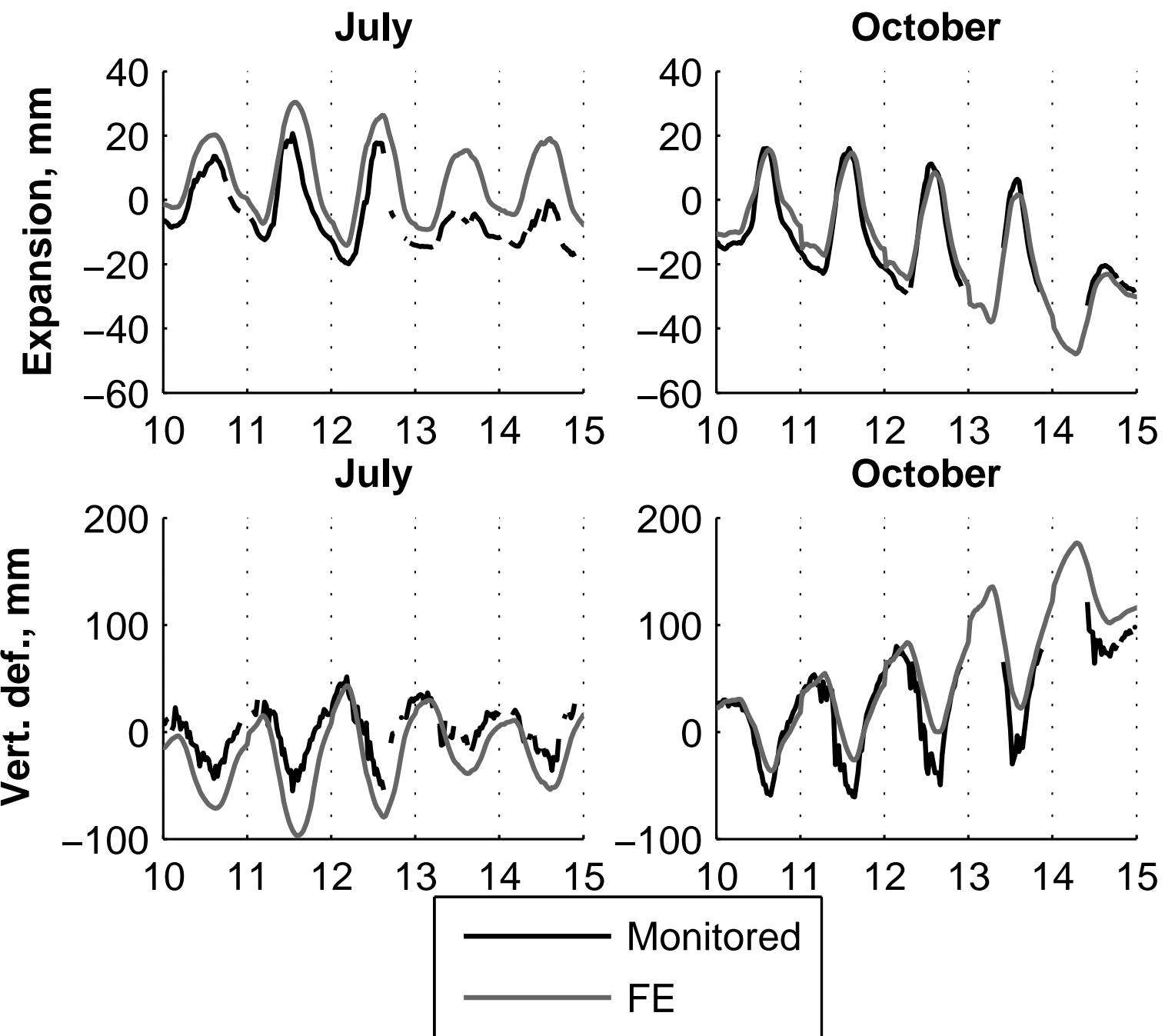


Figure 7

[Click here to download Figure: f_7b.eps](#)

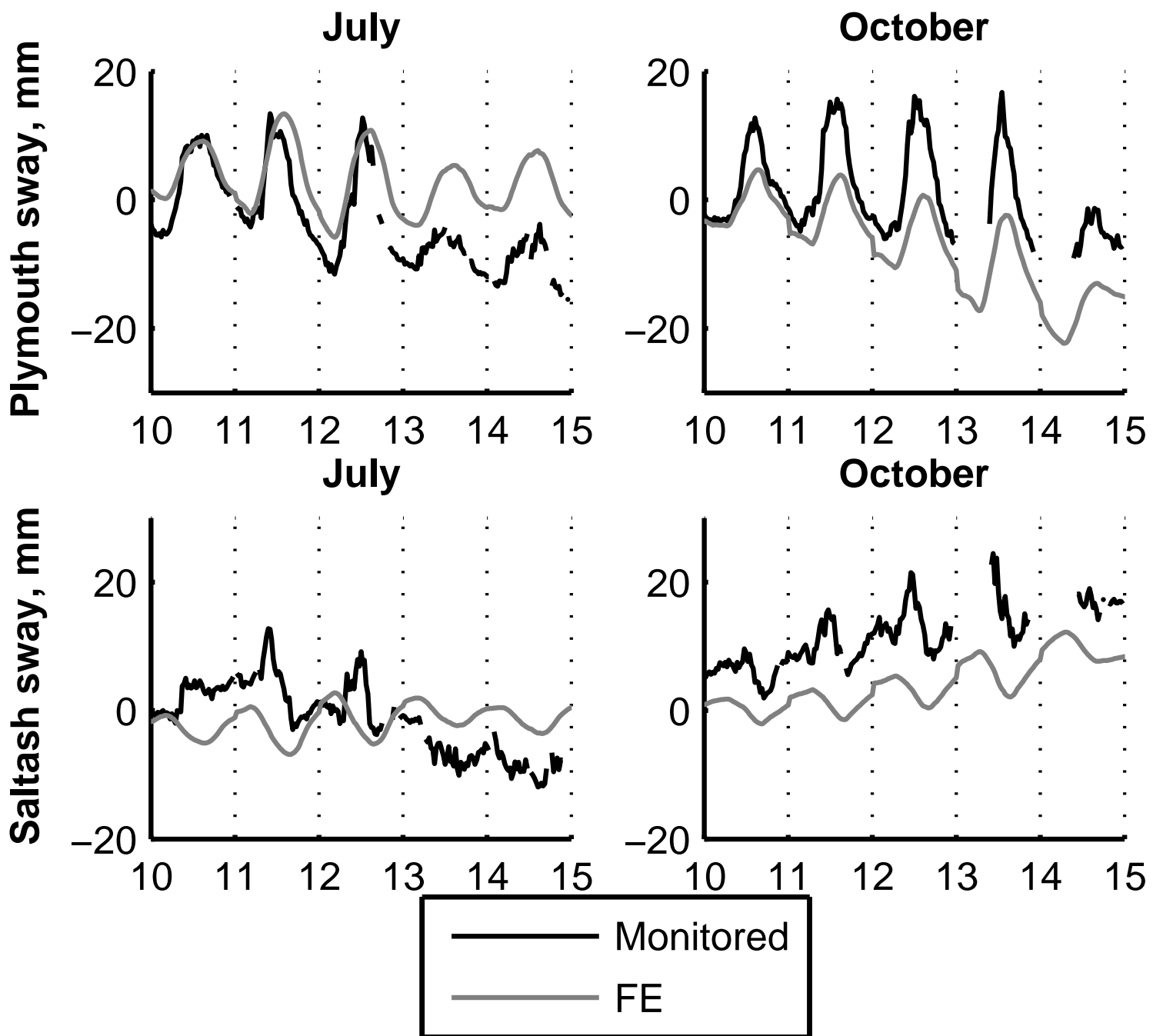


Figure 8
[Click here to download Figure: f_8b.eps](#)

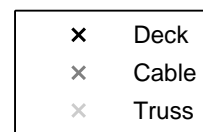
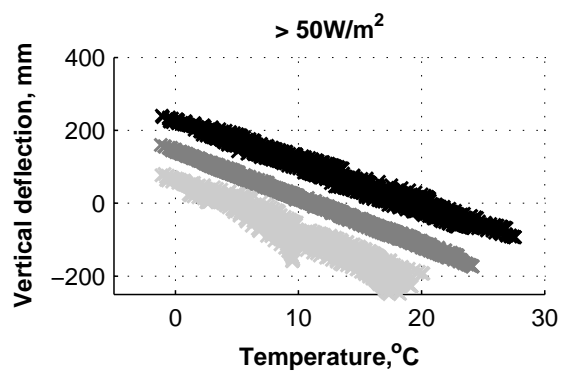
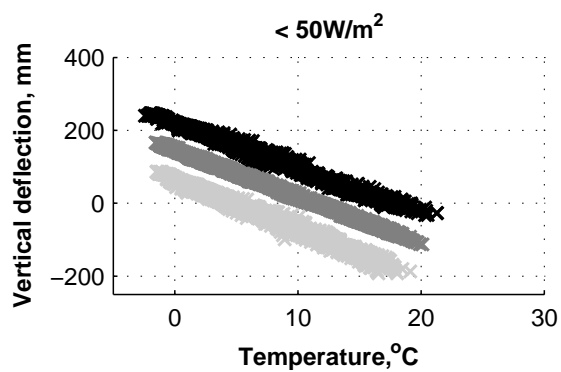
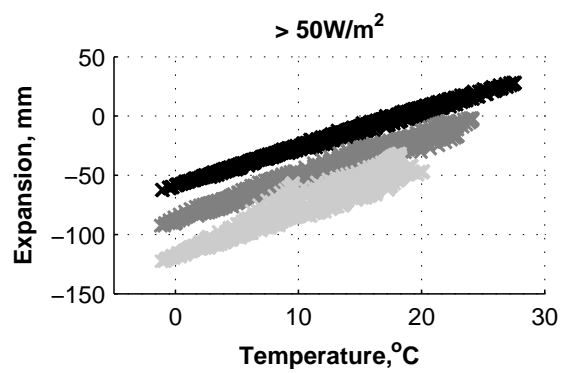
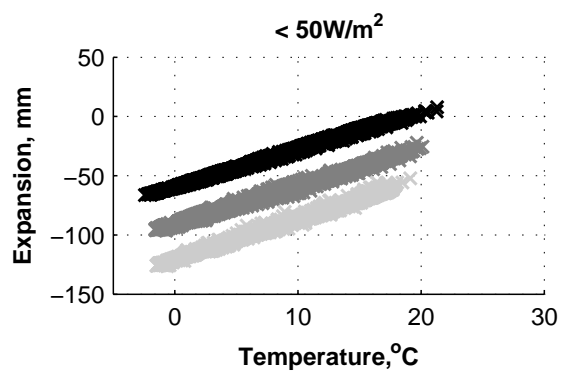


Figure 9

[Click here to download Figure: f_9b.eps](#)

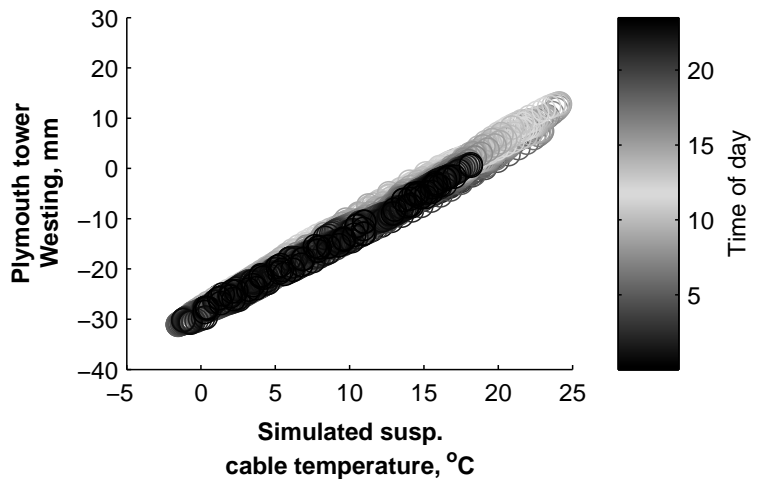
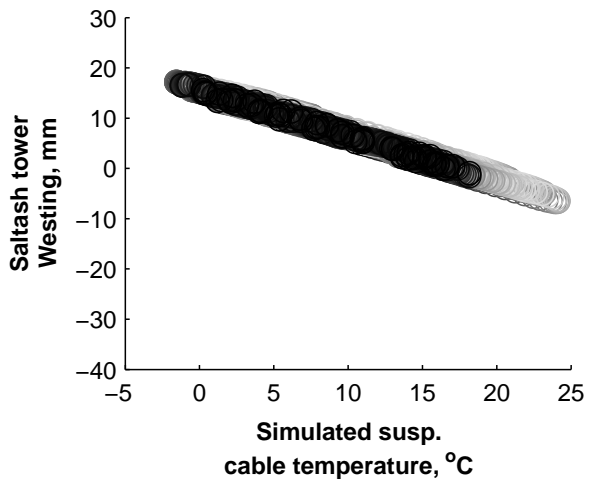
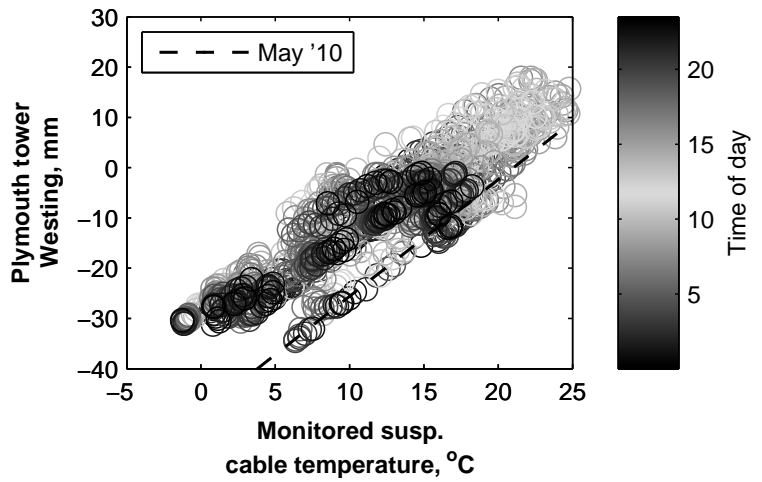
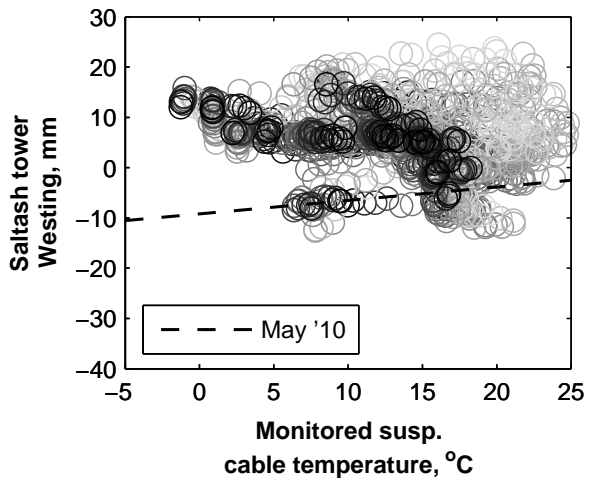


Figure and Table captions

Figure 1: Dimensions, stay cable layout and sensor layout for Tamar Bridge.

Figure 2: Monitored temperature time series, centred on two dates. Top: January 10th 2010 (cloudy sky). Bottom: July 8th 2010 (clear sky)

Figure 3: Comparison between airport-monitored and predicted cloud cover

Figure 4: Finite Element model of Tamar Bridge. Top: Structural and thermal conduction elements. Bottom: Solar radiation and convection elements.

Figure 5: Monitored and simulated bridge temperature time series. Top left: Cable temperature in July. Top Right: Cable temperature in October. Middle left: Deck temperature in July. Middle right: Deck temperature in October. Bottom left: Tower temperature in July. Middle right: Tower temperature in October.

Figure 6: Monitored and simulated time series for bridge displacements at midspan. Top left: Longitudinal expansion in July. Top Right: Longitudinal expansion in October. Bottom left: Vertical deflection in July. Bottom right: Vertical deflection in October.

Figure 7: Monitored and simulated time series for spanwise sway of the tops of the main towers (positive values move West). Top left: Plymouth tower in July. Top Right: Plymouth tower in October. Bottom left: Saltash tower in July. Bottom right: Saltash tower in October

Figure 8: Simulated deflections at mid-span (CG062) vs. Temperatures from FE model, separated by levels of solar radiation. Top left: Spanwise expansion on samples below 50W/m². Top right: Spanwise expansion on samples above 50W/m². Bottom left: Vertical deflection on samples below 50W/m². Bottom right: Vertical deflection on samples above 50W/m².

Figure 9: Time dependence of tower deflection vs. Suspension cable temperature. Top row: Monitored. Bottom row: FE Simulated. Left column: Saltash tower. Right column: Plymouth tower.

Table 1: Typical heat transfer properties

Table 2: Coefficients determined from response surface models predicting bridge displacements at midspan.